EXPERIMENTAL STUDY OF THE DYNAMIC STABILITY OF THE EXOMARS CAPSULE

A. Gülhan[(1)], J. Klevanski[(1)], S. Willems[(1)]

[(1)] Supersonic and Hypersonic Technology Department of the Institute of Aerodynamic and Flow Technology, German Aerospace Research Center (DLR), Linder Höhe, D-51147 Cologne, Germany, Email: Ali.Guelhan@dlr.de, Josef.Klevanski@dlr.de, Sebastian.Willems@dlr.de

ABSTRACT

Damping derivatives of the Exomars capsule have been measured using free oscillation technique in the Trisonic Windtunnel TMK. A cross flexure instrumented with strain gauges measured the dynamic motion of the model in a Mach number range from 1.8 to 3.5. Reynolds number and angle of attack of the capsule were also varied during experiments. The results show a strong dependency of damping derivatives on the Mach number and angle of attack. Compared to the laminar flow on the smooth surface roughness induced transition seems to effect the dynamic stability of the vehicle remarkably.

1. INTRODUCTION

Dynamic stability has been one of the major critical issues of entry flights with capsule configurations. Several studies showed the shortcomings of the CFD simulation but also discrepancies between different measurement techniques [1], [2], [3] and [4].
The aerodynamic behavior of the EXOMARS capsule during its entry into the Martian atmosphere is a very important parameter for the success of the mission. In particular the dynamic stability of such configurations in transonic and supersonic flight regimes is critical. The prediction of the dynamic stability using both experimental and CFD tools is quite challenging and requires reliable data on the static stability behavior of the vehicle. Therefore in addition to the existing static stability data dynamic stability tests have been carried out in the DLR Trisonic Windtunnel Cologne in a Mach number range of 1.8 to 3.5.

2. EXPERIMENTAL TOOLS

The windtunnel model has a diameter of 100 mm. The front part of the model is made out of an Aluminium alloy. The rear part of the model is made out of copper. Additional modular tungsten parts are used to move the center of gravity of the model. The model allows also changing moment of inertia by replacing some tungsten parts with other elements. In order to simulate the real flight configuration the spring cavities on the rear surface of the vehicle were also considered (Figure 1).

For correct measurements it is very important to minimize the deviation between the center of gravity (CoG) and the center of rotation (CoR).

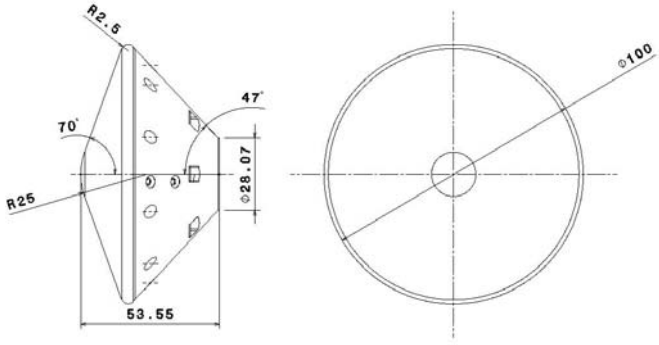

Figure 1: EXOMARS model for dynamic stability measurements

A sketch of the model configuration with integrated instrumentation for the free oscillation tests is shown in Figure 2.

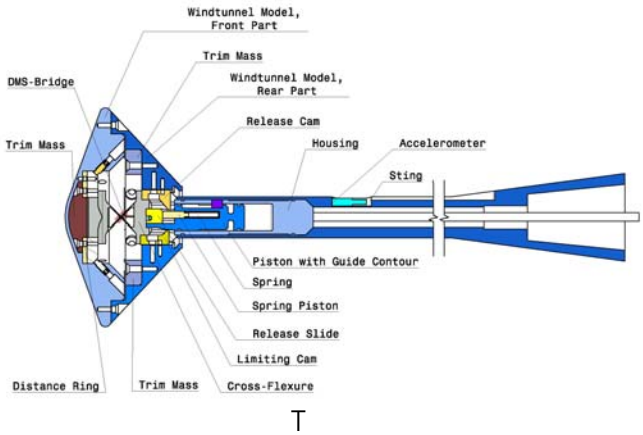

Figure 2: Model configuration of TMK dynamic stability tests

The key element of the measurement technique is the elastic cross-flexure. It is designed to provide the necessary motion around the CoR, (CoR is as close as possible to CoG).
The stiffness of the cross-flexure was defined by considering the duplication requirement with respect to the reduced frequency in addition to Mach and

Proc. of '7th European Symposium on Aerothermodynamics', Brugge, Belgium 9–12 May 2011 (ESA SP-692, August 2011)

Reynolds numbers duplication. The cross flexure should also allow to get about 20 oscillation cycles for 5 different releases during one run. The cross-flexure is made out of a special steel alloy. The EXOMARS model with the integrated cross-flexure is mounted to the sting, which contains the pneumatic release mechanism. The initial amplitude of the oscillation is defined by a release cam. The same system allows also catching the model and stopping the oscillation. The control of the model releasing and catching is provided by a special software in LabView-version.

The cross-flexure is equipped with special strain gauges. The strain gauges were connected to a Wheatstone bridge. The measured DMS-voltage signal corresponds to the deflection angle θ of the cross-flexure. The sting is made out of a steel alloy. It is designed to minimize the interaction with wake: The sting length - model diameter ratio is above 3.55 ($L_{sting}/D_{ref} > 3.55$) and sting diameter - model diameter ratio is less than 0.18 ($D_{sting} / D_{ref} < 0.18$). The model configuration for dynamic stability measurement in TMK is shown in Figure 3.

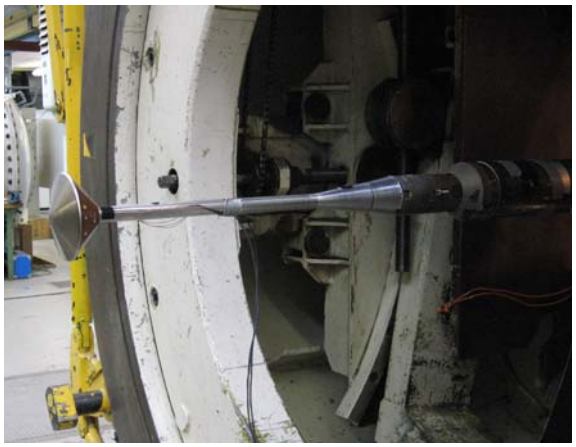

Figure 3: EXOMARS model for dynamic stability measurements in TMK

3. CALIBRATION OF THE CROSS FLEXURE

3.1. Static calibration

The cross-flexure stiffness and the calibration factor of the DMS for the measurement of deflection angle is determined by the static calibration performed with the special static calibration device, which is fixed to the special movable support (see Figure 4).

The mechanical moment is produced by placing of the etalon masses on the several pre-defined positions of the horizontal bar of the calibration device (Figure 4). The resulted deflection of the calibration device due to the cross-flexure deformation is compensated by the rotation of the support sting. The horizontal orientation of the horizontal bar was restored and the compensating angle of the support equals exactly to the cross-flexure deformation. The compensation angle of the support is measured with both electronic sensors and by the spirit level. The electrical output signal of the DMS is also measured.

Figure 4: Static Calibration Device

After compensation of the Zero-deviation the linear regressions for DMS calibration were performed. The mechanical stiffness (as a linear regression) for the cross-flexure is shown in Figure 5. Static calibration leads to a cross flexure stiffness of C_y = 4.46 Nm/rad.

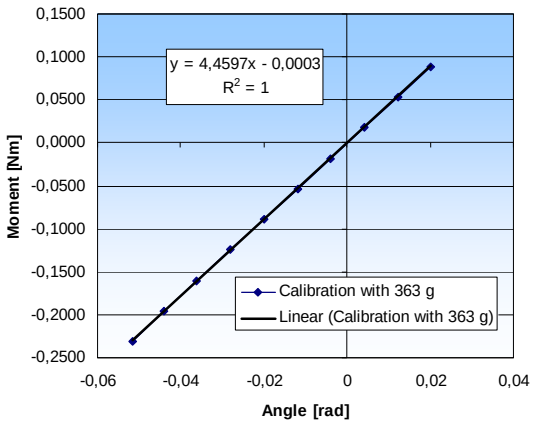

Figure 5: Static calibration curve

3.2. Dynamic calibration

The main objectives of the dynamic calibration are to estimate the moment of inertia of the wind tunnel model I_y and the damping characteristic of the flexure without flow $k_y(\omega)$.

For this task a specially designed dynamic calibration device was used (see Figure 6). It has special catches for the etalon disks, with the known geometry and inertia characteristics. This device is fixed to the cross-flexure and both are mounted to the sting which contains the release mechanism. The free oscillations are initiated via this release mechanism.

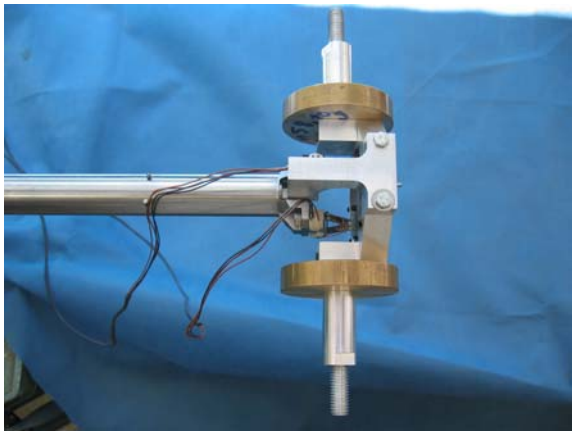

Figure 6: Dynamic Calibration Device

The moment of inertia was estimated from the dynamic calibration curves shown in Figure 7. The linear regression was used to describe the dependency of the moment of inertia on the frequency, i.e. $I_{y\ Disc\ Comb} = f(1/\omega^2)$ (see deep blue line in Figure 7).
The regression coefficients 4.449 correlates very well with the value coming from the static calibration of the cross-flexure (c_y=4.46). The regression shift corresponds very well to the moment of inertia of the dynamic calibration device:

$$I_{y\ Device} = 6.87972\text{E-}05\ \text{kg}\cdot\text{m}^2$$

The moment of inertia of the model can be easily calculated as $I_y = c_y/\omega^2 = 0.000459\ \text{kg}\cdot\text{m}^2$

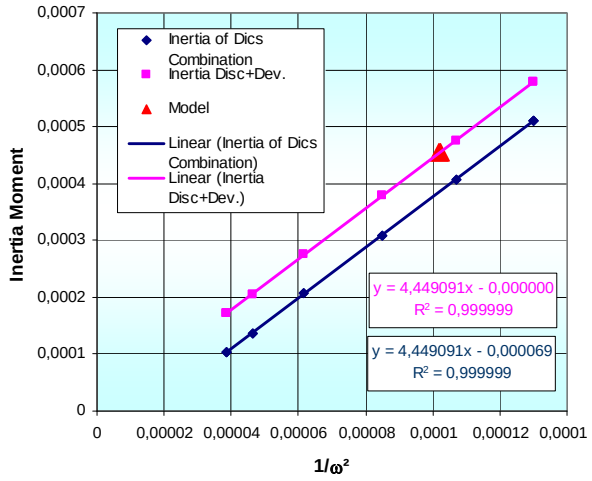

Figure 7: Estimation of the Model Inertia

To check the influence of the atmosphere conditions on the damping the dynamic calibration was carried in the vacuum chamber of the wind tunnel H2K. During the dynamic calibration campaign the special features of the cross-flexure were investigated in details. Very good reproducibility of the data has been noticed for different releases for both cross-flexures.

No amplitude dependency of the damping has been noticed for the cross-flexure. The cross-flexure damping depends on the oscillation frequency (see Figure 8). Therefore the disc combinations are specially defined to cover the necessary frequency range.

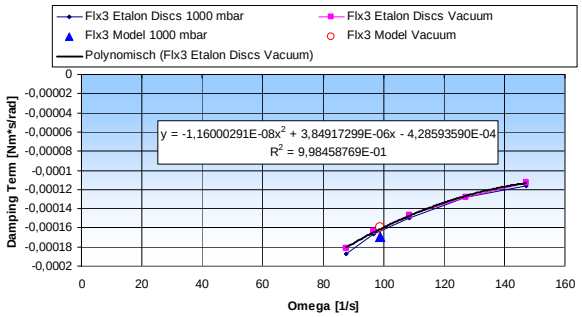

Figure 8: Damping Characteristic of the flexure

The identification method applied for the damping decrement δ and the estimation of the oscillation frequency ω based on the free oscillation tests data processing are described in the section 4.

4. DAMPED OSCILLATION

In TMK the dynamic derivatives of the EXOMARS capsule are estimated via free oscillation method, which analyses free oscillation of the scaled capsule model fixed on a sting by means of a cross flexure with and without supersonic flow. It is to note that in this case it is only possible to estimate the sum of the dynamic derivatives $c_{m\dot{\alpha}} + c_{mq}$ because it is impossible to separate the angle of attack change from the pitch rate due to the kinematical motion limitations by oscillation round the rotation center.

4.1. Basic relations

If we consider the motion of the capsule model fixed on the cross-flexure placed in the flow as the model deflections relative to the trimmed position (under assumption that these deflection are small) we can formulate the differential equation for the free oscillation as:

$$I_y \ddot{\theta} + (k_y + M_{\dot{\theta}})\dot{\theta} + (c_y + M_{\theta})\Delta\theta = 0 \quad (1)$$

where I_y is moment of inertia, k_y is mechanical damping coefficient, c_y represents mechanical stiffness coefficient, $M_{\dot{\theta}}$ is aerodynamic damping and M_{θ} is aerodynamic stiffness, $\Delta\theta$ represents here the deflection angle. In case of the flow parallel to the sting axis deflection angle equals to the angle of attack:

$$\phi = 0; \qquad \theta = \alpha\,.$$

The first term $I_y \ddot{\theta}$ represents the inertia; the second term $(k_y + M_{\dot{\theta}})\dot{\theta}$ represents damping and the third term $(c_y + M_\theta)\theta$ the elasticity.

If the capsule model is placed in vacuum (no flow influence, aerodynamic damping $M_{\dot{\theta}} = 0$ and aerodynamic stiffness $M_\theta = 0$) then the equation 1 can be written as:

$$I_y \ddot{\theta} + k_y \dot{\theta} + c_y \theta = 0 \quad (2)$$

The ansatz for the analytic solution for the damped harmonic oscillation (basic solution of the equation 1) is:

$$\theta = \hat{\theta}\, e^{-\delta t} e^{i\omega t} \quad (3)$$

Here $\hat{\theta}$ represents the oscillation amplitude and δ represents the oscillation decrement.
The first derivative of $\theta(t)$ is:

$$\dot{\theta} = \hat{\theta}\, e^{-\delta t} e^{i\omega t}(-\delta + i\,\omega) \quad (4)$$

and the second derivative of $\theta(t)$ yields:

$$\ddot{\theta} = \hat{\theta}\, e^{-\delta t} e^{i\omega t}(\delta^2 - 2i\delta\,\omega - \omega^2) \quad (5)$$

Substituting equations 3, 4 and 5 into equation 1 and separation of the real and imaginary part of solution yields:

$$\mathrm{Re}: I_y(\delta^2 - \omega^2) - (k_y + M_{\dot{\theta}})\delta + (c_y + M_\theta) = 0 \quad (6)$$

$$\mathrm{Im}: -I_y 2\delta + (k_y + M_{\dot{\theta}}) = 0 \quad (7)$$

From equations 6 follows:

$$(c_y + M_\theta) = -I_y(\omega^2 - \delta^2) \quad \text{with} \quad \delta << \omega \quad (8)$$

and

$$\omega_{va} = \sqrt{-\frac{c_y}{I_y}}; \qquad \omega_{wt} = \sqrt{-\frac{c_y + M_\theta}{I_y}} \quad (9)$$

From equations 7 yields:

$$(k_y + M_{\dot{\theta}}) = 2I_y\,\delta \quad (10)$$

Assuming the damping decrement δ and the oscillation frequency ω are determined with and without of flow influence and mechanical damping k_y, mechanical stiffness c_y of the cross-flexure and the inertia moment of the capsule model I_y are known, we can easily calculate both the aerodynamic stiffness and the aerodynamic damping:

$$M_\theta = -I_y\omega_{wt}^2 - c_y = I_y\left(\omega_{va}^2 - \omega_{wt}^2\right) \quad (11)$$

$$M_{\dot{\theta}} = 2I_y\delta_{va} - k_y \quad (12)$$

Finally the dimensionless derivatives can be calculated using following relations:

$$c_{m\alpha} = M_\theta \Big/ \left(\frac{\rho}{2} u_\infty^2 S_{ref}\, D_{ref}\right) \quad (13)$$

$$\left(c_{m\dot{\alpha}} + c_{mq}\right) = 2\,u_\infty\, M_{\dot{\theta}}\left(\frac{\rho}{2} u_\infty^2 S_{ref}\, D_{ref}^2\right) \quad (14)$$

The stiffness c_y and the mechanical damping k_y of the cross-flexure and the inertia moment of the capsule model I_y is estimated via static and dynamic calibration tests.

4.2. Calculation of the damping decrement

The damping decrement δ and the free oscillation frequency ω are calculated on basis of the recorded oscillation data as the nonlinear regression model parameters via special identification routine **R2LIN** from the **IMSL**-library, based on the mean square method [8].

The nonlinear regression model is in general case

$$y_i = f(x_i, \theta) + \varepsilon_i i, \quad i = 1,2,...,n \quad (15)$$

where the observed values of the y_i's constitute the responses or values of the dependent variable, the x_i's are the known vectors of values of the independent (explanatory) variables, f is a known function of an unknown regression parameter vector θ, and the ε_i's are independently distributed normal errors each with mean zero and variance σ^2.

For this model, a least squares estimate of θ, is also a maximum likelihood estimate of θ,. The residuals for the model are:

$$e_i(\theta) = y_i - f(x_i, \theta) = y_i - (\theta_1 e^{\theta_2 t_i}\cos(\theta_3 t_i + \theta_4) + \theta_5) \quad (16)$$

A value of θ that minimizes

$$\sum_{i=1}^{n} [e_i(\theta)]^2 \Rightarrow \min \quad (17)$$

is a least squares estimate of θ.

To estimate the values of θ, which correspond to the minimum, the equation 17 is to partially differentiate, set to 0 and to solve with respect to θ.

$$\frac{\partial e_i(\theta_k)}{\partial \theta_k} = \frac{\partial(y_i - f(x_i, \theta_k))}{\partial \theta_k} = -\frac{\partial f(x_i, \theta_k)}{\partial \theta_k} = 0 \quad (18)$$

Routine **R2LIN** is designed so that these residuals are input one at a time from a user-supplied subroutine. This permits **R2LIN** to handle the case when n is large and the data cannot reside in an array but must reside on some secondary storage device.

Routine **R2LIN** is based on MINPACK routines LMDIF and LMDER by Moré et al. (1980). The routine **R2LIN** uses a modified Levenberg-Marquardt method to generate a sequence of approximations to a minimum point.

For the damping harmonic oscillation solution ansatz (equation 3) the nonlinear regression can be written in form:

$$y_i = \theta_1 e^{\theta_2 t_i} \cos(\theta_3 t_i + \theta_4) + \theta_5 \qquad (19)$$

If we compare nonlinear regression 19 with ansatz 3 we conclude that:

$$\hat{\theta} = \theta_1; \qquad \delta = \theta_2; \qquad \omega = \theta_3 \qquad (20)$$

To improve the iteration convergence of the **R2LIN** the nondefault convergence parameters preliminary established with the special **R8LIN** routine are used.

The correct choose of the initial values of $\theta_1 \ldots \theta_5$ is very important for the iteration convergence of the routine **R2LIN**. To improve the iteration convergence the data pre-processing will performed. The useable regions of data will be chosen. For these regions the mean values will be estimated. Mean is used as the initial value for θ_5. Based on the preliminary established local minimum/maximum values the initial values for amplitude θ_1 and for frequency θ_3 and will be estimated. The initial value for the phase shift θ_4=0, because the start and end points of the regions corresponds to the local minimums/maximums. The damping decrement θ_2 will be initially set to 0.

Figure 9 shows the original (measured) data in comparison with the data reconstructed by regression 19 and demonstrates the high quality of the reconstruction.

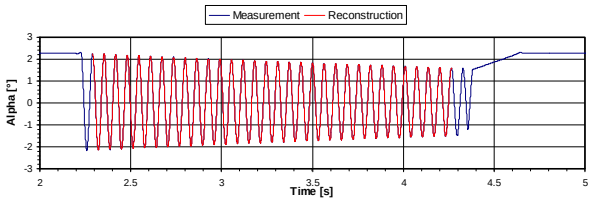

Figure 9: Original Measurement Data(blue) and Reconstructed Data(red)

4.3. Possible error sources

A possible deviation between the Model Aerodynamic Reference Point (RP) and the Center of Rotation (CoR) could cause some error in the data on the pitch coefficient (Figure 10).

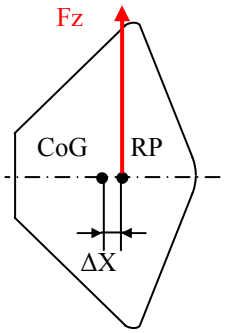

Figure 10: Schema : Influence of No Coincidence of the RP and the CoR

The non-coincidence of the RP and of the CoR in the axial direction ΔX results in an additional pitch moment, caused by the normal aerodynamic force:

$$\Delta c_m(\alpha) = c_{za}(\alpha)\frac{\Delta X}{D_{ref}}$$

Possible discrepancy between the Reference Point and the CoR is less than 0.3 mm: $\Delta X \leq \pm 0.3$ mm. The influence of the mismatch between the RP and the CoR of ΔX = -0.3 mm on the moment characteristic $c_m(\alpha)$ is shown in the Diagrams Figure 11. As shown in the figure there is a small effect, which cannot explain the remarkable difference between pitch static coefficient derivatives ($c_{m\alpha}$) measured by static aerodynamic tests and damping derivatives tests. The $c_{m\alpha}$ values estimated by the free oscillation method are ca. 30% to 50% higher than the values gained on basis of the static tests.

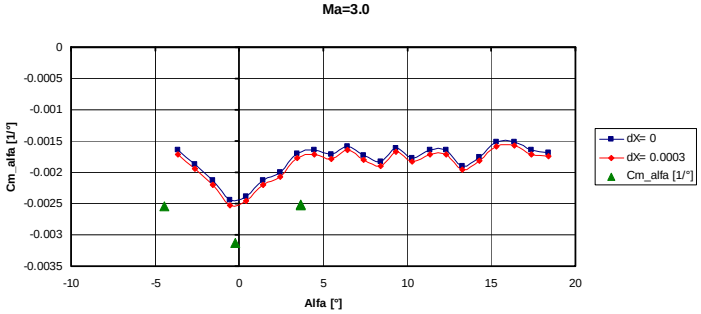

Figure 11: Momentum Characteristic of the EXOMARS Capsule $C_{m\alpha}$

The sting elasticity results in an additional degree of freedom of the investigated oscillation of the EXOMARS capsule model. During the wind tunnel test campaign the acceleration of the sting was measured with an accelerometer. It was integrated into the sting about 100 mm downstream of the model CoR (see Figure 2). The calculated sting eigenvibrations

frequency is about $f \approx 40$ Hz (nearby double frequency of the Exomars capsule model eigenvibrations). The accelerometer data just after the model release is strongly influenced by the model high acceleration caused during release process. This effect becomes weak within a short time.

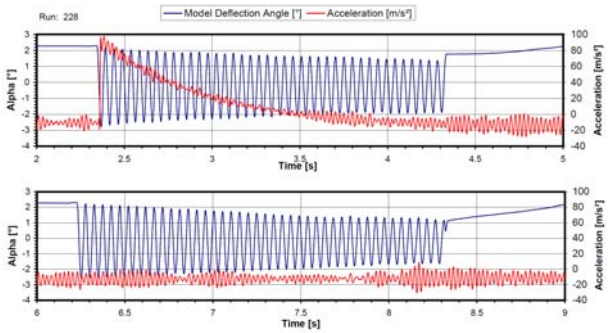

Figure 12: Model Deflection Angle and Accelerometer History (Run 228)

Fast Fourier Transformation (FFT) was used for analysis of the interference between the model angular deflection and the elastic sting motion for the model angular histories and for the sting acceleration history without flow (Run 227) and with flow (Run 228).

The analysis of the amplitude distribution in the frequency spectrum shows that the model angular oscillations have an influence on the sting motion: Both the spectrums lines have an extremum by the model oscillation eigenfrequency (Run 227: $\omega \approx 98.6$ 1/s without flow, Figure 13 and Run 228: $\omega \approx 129.6$ 1/s with flow, Figure 14). This influence is significant especially under flow condition (Run 228).

On the contrary the sting eigenvibrations have no significant influence on the model angular oscillation: The second extremum by the sting oscillation frequency ($\omega \approx 256$ 1/s without flow, Figure 13 and $\omega \approx 251$ 1/s with flow, Figure 14) does not reflect in the model angular motion spectrum.

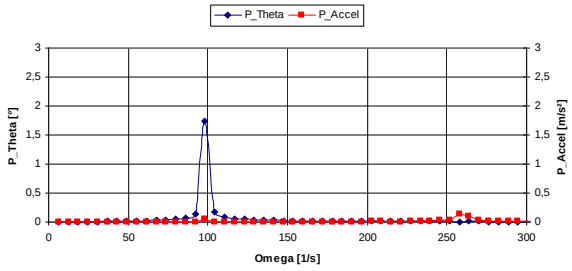

Figure 13: Amplitude-Frequency Spectrum (Run 227, w/o Flow)

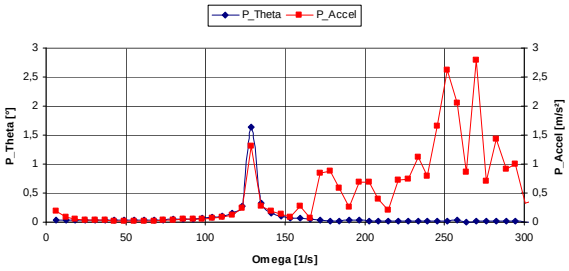

Figure 14: Amplitude-Frequency Spectrum (Run 228, with Flow)

5. FLOW PARAMETERS

For the duplication of the flight Reynolds number the ejector operation mode of TMK was used. The ejector mass flow rate tuned in such a way that the flight Reynolds number based on the model diameter of 0.1 m was set to approx. 1.10^6. The flow parameters computed from the measured reservoir pressure and total temperature with the known nozzle geometry, i.e. Mach number are listed in Table 1.

Ma [–]	p_1[bar]	u_1 [m/s]	q [bar]
1.8	0.1330	482.0	0.3017
1.9	0.1332	498.2	0.3366
2	0.1052	512.6	0.2947
2.2	0.0901	539.7	0.3053
2.5	0.0655	573.5	0.2867
3	0.0369	617.5	0.2328
3.5	0.0246	650.2	0.2112

Table 1: Flow parameters of TMK tests

6. EXPERIMENTAL RESULTS

6.1. Tests at different angles of attack

The results of several experiments at different angles of attack are shown in Figure 15. At an angle of attack of 1° the capsule is stable for Mach numbers higher than 2.5, unstable for mach numbers below 2.5 and indifferent for Mach 2.5. The Mach range with stable capsule behaviour is same as with 0° angle of attack, but the configurations are always more stable, especially at low Mach numbers. At Mach 1.8 and an angle of attack of 1.5° the capsule becomes stable. There is nearly no difference between 2.0° and 4.0° angle of attack at Mach 1.8. At angle of attack of 4° a damped oscillation was noticed for all tested Mach numbers (1.8 to 3.5). The results show a strong dependency of the pitch damping derivative on the angle of attack is much higher than expected.

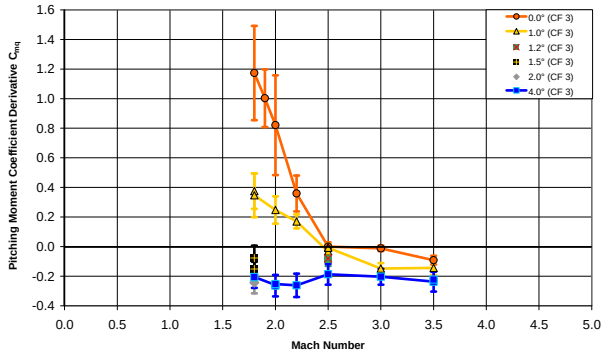

Figure 15: Pitch damping coefficient derivative for different angles of attack

6.2. Tests with surface roughness

For boundary layer tripping a defined surface roughness was applied to the capsule front surface. With rough surface the capsule becomes a little bit more stable (but still unstable) below Mach 2.5. But it becomes unstable above Mach 2.5. This can be seen in Figure 16.

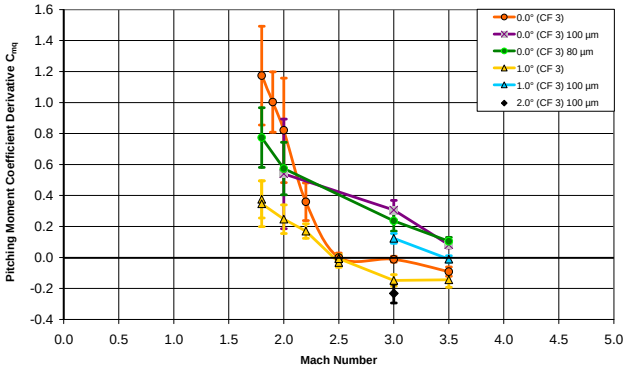

Figure 16: Pitch damping coefficient derivative for different surface roughnesses

There is no significant difference between a surface roughness of R_a = 100 μm and a surface roughness of of R_a = 80 μm. Again an angle of attack beyond 1° results in a more stable configuration. For example at Mach 3.0 an angle of attack of 2° results in a stable configuration even with a surface roughness of of R_a = 100 μm.

Schlieren pictures of the wake flow were very useful to analyse the wake flow. For all tests a well established flow field has been observed. In addition, in order to compare the wake flow, which dominates the dynamic stability behavior of the capsule, Schlieren pictures of different test configurations have been compared using the wake flow size described with the parameters shown in Figure 17.

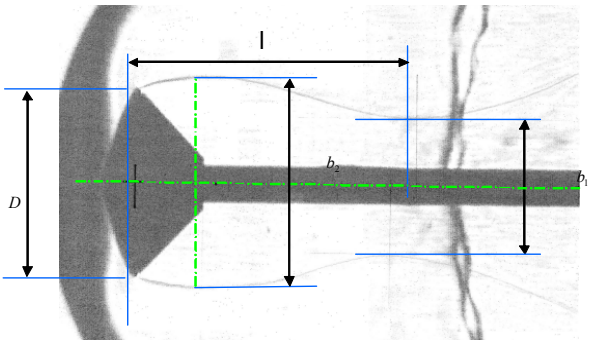

Figure 17: Characteristics of the wake flow

Measured wake flow geometry parameters with corresponding pitch derivative coefficient are listed in Table 2.

surface	Ma	2.0	3.0	3.5
smooth	b_2/D	1.09	0.95	0.93
	l/D	n.m.	1.19	1.21
	c_{mq}	0.821	-0.012	-0092
rough	b_2/D	1.11	0.98	0.95
	l/D	n.m.	1.16	1.18
	c_{mq}	0.574	0.236	0.104

Table 2: Wake size depending on the Mach number and surface property

The parameter b_1/D was difficult to measure accurately and therefore is not included in the table.
The data of tests on smooth surface shows that the wake diameter decreases by increasing the Mach number. Since a clearly measurable dependency of the wake diameter (b_2/D) and pitch derivative (c_{mq}) on the Mach number has been noticed, a remarkable change of the flow topology around the capsule edge is expected. Therefore the geometry of the capsule cone edge seems to be an important parameter to influence the dynamic stability of the vehicle.
For the rough surface a similar dependency of b_2/D and c_{mq} on the Mach number has been measured. But the sensitivity is weaker. Although b_2/D gets bigger compared to the smooth surface case, the capsule becomes unstable at Mach numbers between 2.5 and 3.5.
A Reynolds number increase seems to cause similar effects like the application of surface roughness, since both measures lead to boundary layer transition and turbulent flow on the front surface of the capsule.

7. CONCLUDING REMARKS

The main results of the test campaign with respect to the dynamic stability of the EXOMARS capsule can be summarized as follows:

- At angle of attack below 1° the Exomars capsule with a smooth surface is dynamically stable at Mach numbers above 2.5.
- At 4° angle of attack the Exomars capsule with a smooth surface is dynamically stable at Mach numbers between 1.8 and 3.5.
- Tripping the boundary layer flow on the front surface changes the dynamic stability behaviour of the capsule significantly.
- At flight Reynolds number and angles of attack below 1° the Exomars capsule with a rough surface, i.e. tripped boundary layer flow becomes dynamically unstable for Mach numbers between 1.8 and 3.5.
- TMK data with the rough surface, i.e. tripped boundary layer show similar tendency as to the ISL free flight data. Both results show that the capsule with a rough surface, i.e. turbulent flow on the front surface is dynamically unstable even at Ma=3. But the flow around the capsule will laminar during the flight.
- Schlieren pictures show that during tests with the smooth surface at flight Reynolds number the wake flow diameter increases by decreasing the Mach number and results in higher dynamic pitch instability. Since a clearly measurable dependency of the wake diameter (b_2/D) and pitch derivative (c_{mq}) on the Mach number has been noticed, a remarkable change of the flow topology around the capsule edge is expected. Therefore the geometry of the capsule cone edge seems to be an important parameter to influence the dynamic stability of the vehicle.
- For the rough surface a similar dependency of the wake size (b_2/D) and c_{mq} on the Mach number has been measured. But the sensitivity is weaker. Although b_2/D gets bigger compared to the smooth surface case, the capsule becomes unstable at Mach numbers between 2.5 and 3.5.

8. ACKNOWLEDGEMENTS

The authors express their special acknowledgement to the European Space Agency (ESA), Thales-Alenia-Italy and Fluid Gravity for their financial and technical support.

9. REFERENCES

[1] Cheatwood F. McNeil, Winchenbach Gerald L., Hathaway Wayne, Chapman Gary; *Dynamic Stability Testing of the Genesis Sample Return Capsule*, AIAA-2000-1009.

[2] Schoenberger Mark, Hathaway Wayne, Yates Laslie, Desai Presun; *Ballistic Range Testing of the Mars Exploration Rover Entry Capsule*, AIAA-2005-0055

[3] Murman Scott M., Aftosmis Michael J.; *Dynamic Analysis of Atmospheric-Entry Probes and Capsules*, AIAA-2007-0074.

[4] Edquist K. T., Desai P. N., Schoenenberger M.; *Aerodynamics fort he Mars Phoenix Entry Capsule*, AIAA 2008-7219.

[5] Esch, B.; *Bestimmung instationärer Derivativa im Hyperschall mit Hilfe der Methode der freien Oszillation*, Diplomarbeit RWTH

[6] Esch, H.; *Die 0.6-m x 0.6-m-Trisonische Meß-strecke (TMK) der DFVLR in Köln-Porz*, DFVLR-Mitt. 86-21, März, 1986.

[7] Gülhan, A., Tarfeld, F., Achner, M.; *Static Stability Tests on the EXOMARS Capsule in the DLR Trisonic Windtunnel TMK DLR*, Report DLR-EXOMARS-SS-TMK-TR.

[8] IMSL. Fortran Subroutines for Statistical Applications. Stat Library Volume 1

[9] Murman, S.; Aftosmis, M.; *Dynamic Analysis of Atmospheric-Entry Probes and Capsules*, AIAA 2007-0074, January, 2007.

[10] Berner, C., Brenker, S., Sommer, E.; *EXOMARS Phase B1-Extension, ISL Open Range Free Flight Tests*, Final Report / Phase 2 Additional Tests.